



Cite this: DOI: 10.1039/c4ce01869a

New growth modes of molybdenum oxide layered 1D structures using alternative catalysts: transverse mode vs. axial mode†

Tao Sheng,^a Baobao Cao,^{bc} Yong Zhang^d and Haitao Zhang^{*b}

Different from the common metal catalysts (e.g., Au) employed in catalyst-assisted growth of one-dimensional (1D) structures, a variety of molybdenum oxide (MoO₃) layered 1D structures were synthesized using a group of alternative alkali metal based catalysts. In contrast to the sole axial growth mode found in conventional catalyst-assisted growth, two different growth modes were observed for the MoO₃ 1D growth here: transverse growth and axial growth. In the transverse mode, the 1D structures grow perpendicularly to the catalyst-deposition axis with the catalyst particles sitting on the side surfaces of the 1D structures; whereas in the axial mode, the growth direction is along the catalyst-deposition axis. The growth modes were explained by a modified vapor–solid–solid (VSS) mechanism, and the factors that affect the growth were explored. Based on the proposed growth mechanism, the growth was extended to a large family of alkali metal based catalysts and hierarchical structures were realized by multiple-growth approaches. This growth mechanism provides a new approach to control the orientation of 1D structures and can be applied to different layered materials.

Received 11th September 2014,
Accepted 4th December 2014

DOI: 10.1039/c4ce01869a

www.rsc.org/crystengcomm

1 Introduction

The vapor–liquid–solid (VLS) process is the most popular vapor-phase method for the controlled growth of various one-dimensional (1D) microstructures and nanostructures with the assistance of catalyst particles. The VLS mechanism was first proposed and developed in the 1960s for the growth of 1D microstructures.¹ With the extensive development of nanotechnology in recent decades, this method has become the most successful and versatile strategy for the synthesis of 1D nanostructures.² Based on a similar catalyst-assisted growth mechanism, different processes analogous to the VLS approach have been further developed, including vapor–solid–solid (VSS),³ solid–liquid–solid,⁴ solution–liquid–solid,⁵ supercritical fluid–liquid–solid,⁶ and supercritical fluid–solid–solid.⁷ The 1D structure growths *via* different processes all

share two fundamental features. (1) Metal or metal alloy particles are usually used to incorporate the source materials. Noble metals and other transition metals, such as Au, Pt, Ag, Ti, Fe, Ni, and Cu, have been commonly used as catalysts.^{2d,3c} Some low melting temperature metals, like Ga, In, and Sn, have been employed as well.^{4c,8} Although non-metal catalysts, like element semiconductors (Ge)⁹ and compounds (Ag₂Se, Ag₂S, Cu₂S, *etc.*),¹⁰ can also be used for the growth of 1D nanostructures, they are relatively less common compared to the metallic catalysts. (2) As the catalyst particles reach a supersaturation state, growth occurs at the catalyst-deposition interface leading to 1D growth along the catalyst-deposition axis, as shown in Fig. 1a. The resulting growth is typically an axial growth no matter if it is a tip growth (model I in Fig. 1a) or a root growth (model II in Fig. 1a) or if the catalyst particles are liquid or solid during the growth.¹¹ Lateral growth (model III in Fig. 1a) of 1D nanostructures has been demonstrated.¹² Although these 1D structures are oriented laterally along the substrate surface, the growth still follows the axial growth mode in which the growth front is the catalyst-deposition interface and the growth direction is along the catalyst-deposition axis.

Orthorhombic molybdenum trioxide (α -MoO₃) has an anisotropic layered structure with strong ionic and covalent bonding within the (010) layers but weak van der Waals interactions between the (010) layers.¹³ α -MoO₃ has potential applications in a wide range of areas including electrochromism and photochromism,¹⁴ lubricants,¹⁵ photocatalysts,¹⁶

^a Department of Physics and Optical Science, and Optical Science and Engineering Program, The University of North Carolina at Charlotte, 9201 University City Boulevard, Charlotte, NC 28223, USA

^b Department of Mechanical Engineering and Engineering Science, The University of North Carolina at Charlotte, 9201 University City Boulevard, Charlotte, NC 28223, USA. E-mail: hzhang3@uncc.edu

^c School of Materials Science and Engineering, Southwest Jiaotong University, No. 111, North 1st Section of Second Ring Road, Chengdu, Sichuan 610031, PR China

^d Department of Electrical and Computer Engineering, The University of North Carolina at Charlotte, 9201 University City Boulevard, Charlotte, NC 28223, USA

† Electronic supplementary information (ESI) available: Additional SEM, EDS, and Raman data, results from control experiments, and UV-vis measurement. See DOI: 10.1039/c4ce01869a

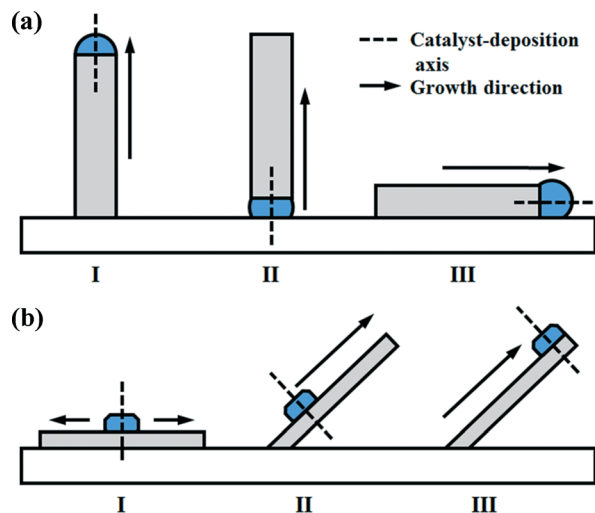


Fig. 1 Comparison of different growth modes for the catalyst-assisted growth of 1D structures. (a) Conventional axial growth mode with tip growth (model I), root growth (model II), and lateral growth (model III). The growth direction for the axial growth mode is parallel to the catalyst-deposition axis. (b) New transverse growth mode with lateral growth (model I) and vertical growth with catalyst particles at different locations along the 1D structures (model II and III). The growth direction for the transverse growth mode is perpendicular to the catalyst-deposition axis.

and gas sensors.¹⁷ Moreover, as a layered hosting material, α - MoO_3 has enabled improved performance of Li-ion¹⁸ and Na-ion batteries.¹⁹ Various MoO_3 nanostructures have been synthesized through solution-based hydrothermal procedures²⁰ and chemical vapor transport/deposition approaches,²¹ including nanowires, nanobelts, nanoflowers, prism-like rods, and nanoribbons. So far, the investigation on the catalyst-assisted growth of MoO_3 1D nanostructures is still rare. The assistance of Au in vapor deposition only altered the orientation^{21f} or served as the preferred nucleation sites²² of the 1D nanostructures rather than promoting the growth of the nanostructures.

In this study, instead of the common metal catalysts, alternative catalysts were employed in the growth of MoO_3 1D structures, including sodium or potassium compounds (*e.g.*, hydroxides, halides, carbonates, *etc.*) and even alkali metal containing substrates (*e.g.*, glass, indium–tin-oxide (ITO) coated glass, and mica). The growth is greatly enhanced by the presence of the catalysts producing 1D structures with different morphologies, including forked nanoplates, extra-long nanobelts, millimeter-long microbelts, and microtowers. The growth mechanism of the 1D structures was identified to be dominated by the VSS process. Most importantly, different from the conventional VSS and similar mechanisms, the 1D growth of MoO_3 here follows two different growth modes: transverse growth and axial growth. The new transverse growth is demonstrated by the growth of MoO_3 nanoplates, nanobelts, and microbelts. In the transverse growth shown in Fig. 1b, the 1D structures grow perpendicular to the catalyst-deposition axis with catalyst particles sitting on different locations (models I–III in Fig. 1b) along the side surfaces of

the 1D structures. On the other hand, the MoO_3 microtowers show conventional axial growth along the catalyst-deposition axis. These growth modes were explained by a modified VSS growth mechanism, and the factors that affect the growth were explored. Based on the growth mechanism, the growth was extended to a large family of alkali metal based catalysts and hierarchical structures were generated using multiple-growth approaches.

2 Experimental

2.1 Reactants and substrates

Molybdenum powder (Mo, Alfa Aesar, 99.9%) was used as the source material for the growth of molybdenum oxide. Different reactants were used as catalytic materials in this study including powders of sodium hydroxide (NaOH, Fisher Scientific, 99.8%), sodium iodide (NaI, Alfa Aesar, 99.9%), potassium iodide (KI, Alfa Aesar, 99.9%), and sodium carbonate (Na_2CO_3 , Alfa Aesar, 99.95%). All reactants were used as received without further processing.

Silicon (100) substrates (p-type, University Wafers) were mainly used in the experiments. The substrates were first cut into 10 mm by 25 mm pieces and ultrasonically cleaned with acetone and ethanol for 15 min (Branson 1510R-MTH, Fisher Scientific), each followed by blow-drying with nitrogen gas. After the above cleaning, the substrate surfaces were hydrophobic. To obtain hydrophilic substrate surfaces, the substrates were then treated with oxygen plasma (Plasma-Preen 862, Kurt J Lesker) for 3 min. For the catalyst-assisted experiments, the hydrophilic Si substrates were drop-cast with NaOH (or KI, Na_2CO_3) solution (54 μL , 10 mM) and air dried in a chemical fume hood. Other alkali ion containing substrates, such as soda-lime-silica glass (microscope slide, Fisher Scientific) and indium tin oxide (ITO) coated glass (Delta Technologies, 25 Ω/\square), were cleaned by the same routine except with the absence of plasma cleaning and subsequent aqueous solution dipping. Mica (Ted Pella, grade V2, #52-25) was cleaved right before growth without other treatment.

2.2 Synthesis

The growths were performed in a home-made hot-wall chemical vapor deposition (CVD) system. The detailed setup has been reported elsewhere.²³ In a typical synthesis, Mo powder was loaded at the center of the reaction chamber with the receiving substrate placed at the downstream. The reaction chamber was first pumped down to ~ 10 mTorr, and then brought up to ~ 200 mTorr with 10 sccm (standard cubic centimeter per minute) O_2 and 10 sccm Ar. The heating temperature at the center was ramped up to 800 $^\circ\text{C}$ in 30 min and lasted for 120 min. Then the heating power was turned off and the chamber was allowed to naturally cool down to room temperature. During the growth, the growth temperature along the substrate was about 620 $^\circ\text{C}$ to 300 $^\circ\text{C}$, according to the temperature profile measured at atmospheric pressure.

2.3 Material characterization

The morphology and composition of the as-synthesized samples were analyzed by scanning electron microscopy (SEM, JEOL JSM-6480) and energy dispersive X-ray spectroscopy (EDS, Oxford Instrument INCA). Crystal structures were characterized using X-ray diffraction (XRD, PANalytical X'pert Pro MRD with Cu K α radiation at $\lambda = 1.5418 \text{ \AA}$) and transmission electron microscopy (TEM, JEOL JEM-2100 LaB₆ operated at 200 kV). Optical measurements were performed using a confocal micro-Raman system (Horiba Scientific, Labram HR800) in backscattering configuration. A laser power of approximately 0.3 mW at 532 nm was used with a 100 \times objective lens. The spectral resolution was about 1 cm⁻¹. Optical absorption spectra were recorded using an ultraviolet-visible (UV-vis) spectrophotometer (Shimadzu, UV2600Plus) in transmission mode. The as-synthesized sample was removed from substrates by ultrasonication in ethanol for 15 s. The dispersion was left for 12 h to ensure enough sedimentation so that the dispersion became transparent under the unaided eye. The dispersion was then transferred into one 10 mm quartz cuvette (Thorlabs, W005654) for absorption measurement.

3 Results and discussion

3.1 Synthesis and characterization of layered 1D structures

1D MoO₃ structures were found to grow over a wide range of substrate growth temperatures from $\sim 525 \text{ }^{\circ}\text{C}$ to $300 \text{ }^{\circ}\text{C}$ for both the growth without catalysts and the growth with NaOH catalysts. Fig. 2 shows a comparison of the morphology

differences between the non-catalyst growth (Fig. 2a) and the catalyst-assisted growth (Fig. 2b–f) with SEM images. For the non-catalyst growth, nanoplates with a rectangular shape were formed with a length of tens of microns, width of several microns, and thickness of hundreds of nanometers. The dimensions of the rectangular nanoplates vary with growth temperatures (shown in Fig. S1 in the ESI†). Typical rectangular nanoplates grown at $\sim 490 \text{ }^{\circ}\text{C}$ with straight edges are shown in Fig. 2a, and the inset shows that the nanoplates have a booklet-like feature consisting of nanometer-thick layers similar to the MoO₃ nanostructures in previous reports.^{22,24} On the other hand, the catalyst-assisted growth resulted in 1D structures with different morphologies. First, the MoO₃ deposition with catalysts yielded a two-tier structure with different ultra-long 1D structures, such as nanobelts (Fig. 2d), microbelts (Fig. 2e), and microtowers (Fig. 2f), grown on top of a dense array of nanoplates (Fig. 2c). This two-tier structure indicates that there are two stages for the catalyst-assisted growth of MoO₃. As shown in Fig. 2b, ultra-long nanobelts (bright features) were grown on top of a nanoplate array (dark background indicated by the square). A close-up view of the nanoplate array in Fig. 2c shows that the nanoplates grown at $\sim 525 \text{ }^{\circ}\text{C}$ with NaOH catalysts have a distinctive forked feature and larger sizes compared to the rectangular ones in Fig. 2a grown without catalysts. Fig. 2d shows ultra-long nanobelts with a length of hundreds of microns up to about one millimeter at the growth temperature of $\sim 490 \text{ }^{\circ}\text{C}$. At the growth temperature of $390 \text{ }^{\circ}\text{C}$, microbelts with a thickness of several microns and a

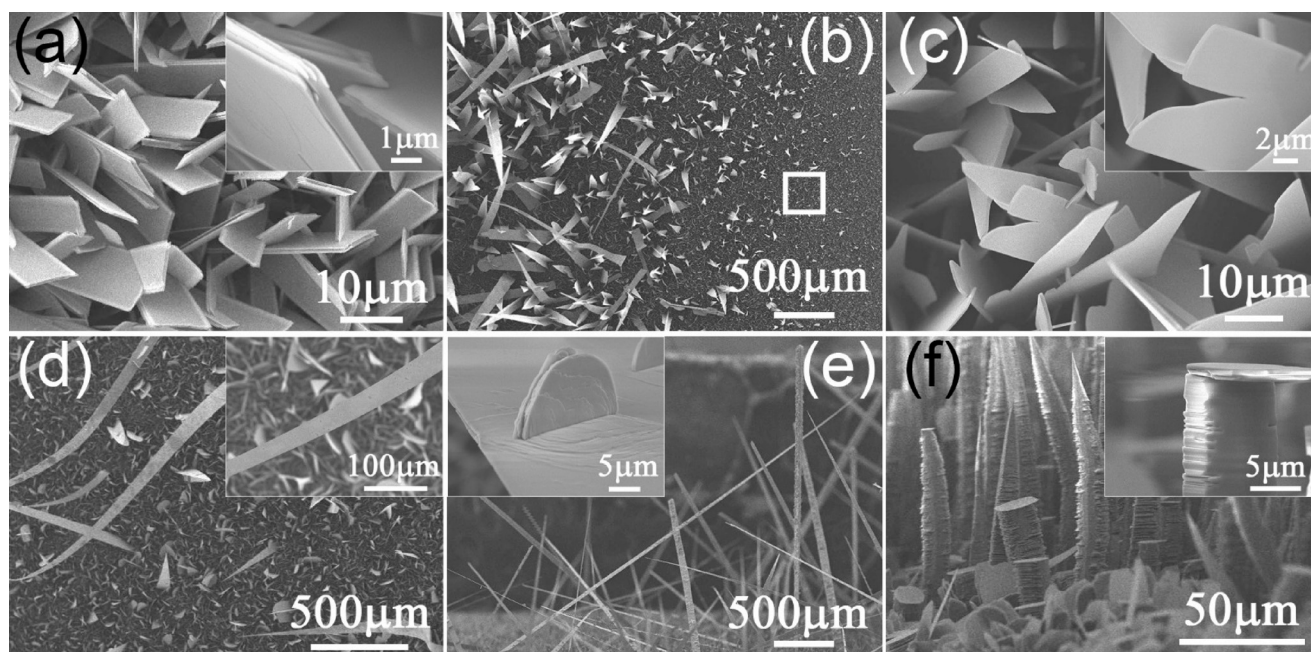


Fig. 2 Effect of alkali metal based catalysts on the morphology of MoO₃ depositions. (a) SEM image of rectangular nanoplates grown at $\sim 490 \text{ }^{\circ}\text{C}$ without any catalysts. (b–f) SEM images of different morphologies grown with NaOH catalysts: (b) nanobelts grown on top of a dense array of nanoplates grown at $\sim 525 \text{ }^{\circ}\text{C}$, (c) close-up view of the forked nanoplates from an area indicated by the square in Fig. 2b, (d) long nanobelts at $\sim 490 \text{ }^{\circ}\text{C}$, (e) side-view of ultra-long microbelts at $\sim 390 \text{ }^{\circ}\text{C}$, and (f) side-view of microtowers at $\sim 300 \text{ }^{\circ}\text{C}$. Insets show detailed features of different MoO₃ structures.

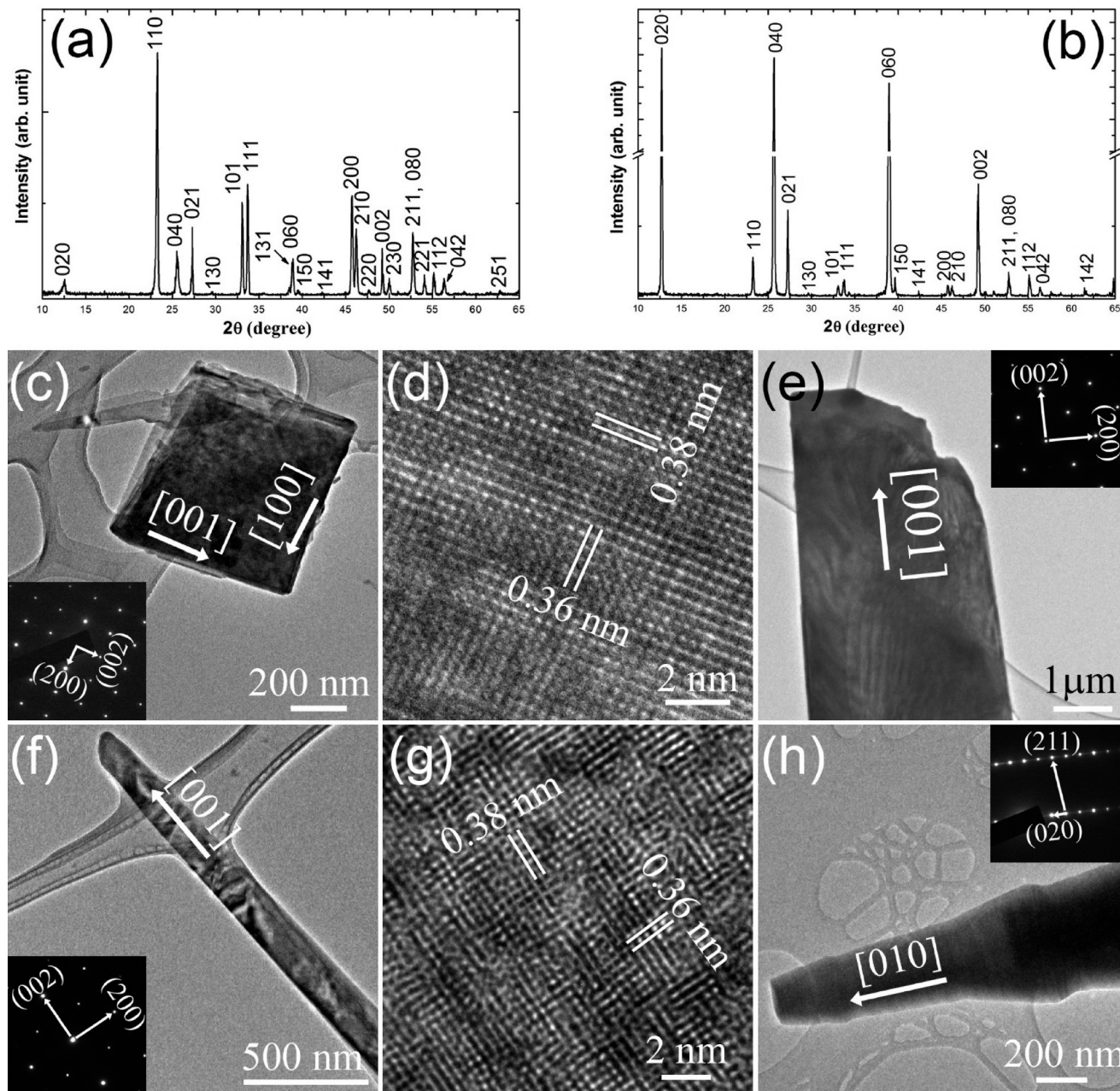


Fig. 3 XRD spectra of (a) a specimen grown without catalysts and (b) a specimen grown with NaOH catalysts. (c) Low-magnification TEM image and (d) HRTEM image of a nanoplate grown without catalysts. (e–h) Various 1D structures grown with NaOH catalysts: low-magnification TEM images of (e) forked nanoplates, (f) nanobelts, and (h) microtowers, and HRTEM image of (g) nanobelts. Insets show SAED patterns of different MoO_3 1D structures.

length of several millimeters appeared with dense circular or semicircular nanoflakes (inset of Fig. 2e) condensed on the side surfaces of the belts. As the substrate growth temperature further decreased to $\sim 300^\circ\text{C}$ at downstream, tower-like structures (Fig. 2f) with micron-sized diameters and lengths were formed at the downstream end of the substrate. The microtowers are stacked structures of quasi-circular layers with tapered tips or flat tops (Fig. 2f and its inset).

The crystal structures of the as-synthesized specimens were characterized by XRD for the non-catalyst growth

(Fig. 3a) and catalyst-assisted growth (Fig. 3b). The XRD patterns for both growths match closely the standard pattern of the orthorhombic $\alpha\text{-MoO}_3$ phase (ICDD PDF # 04-012-8070, $a = 3.9616\text{ \AA}$, $b = 13.8560\text{ \AA}$, and $c = 3.6978\text{ \AA}$). The calculated lattice parameters are $a = 3.963\text{ \AA}$, $b = 13.882\text{ \AA}$, and $c = 3.701\text{ \AA}$ for the non-catalyst growth and $a = 3.967\text{ \AA}$, $b = 13.865\text{ \AA}$, and $c = 3.701\text{ \AA}$ for the catalyst-assisted growth, coinciding with the standard data. No other phases were found in the XRD spectra of both specimens. This result indicates that if there are any catalyst phases present in the catalyst-assisted

specimen, they must be in a very small amount below the detection limit as compared to the amount of the MoO_3 phase. Fig. 3b for the catalyst-assisted growth demonstrates dominant diffraction peaks of (020), (040), and (060) showing a strongly preferred orientation, which may be attributed to the ultra-long 1D structures (Fig. 2d–f) with layered structures oriented preferably parallel to the substrate surface and some nanoplates grown laterally along the substrate surface during the early growth stage (discussed later in the text). The $\alpha\text{-MoO}_3$ phase was also confirmed by TEM on individual 1D structures. Fig. 3c shows a low magnification TEM image of a rectangular nanoplate grown without catalysts and its selected area electron diffraction (SAED) pattern. The nanoplate was exfoliated by ultrasonication in acetone solution to reduce its thickness to get a high-resolution TEM (HRTEM) image, hence the nanoplate was broken into a smaller piece. The SAED pattern in the [010] axis (Fig. 3c) and the HRTEM image (Fig. 3d) show that the nanoplate has a (010) top surface and two orthogonal edges along [100] and [001]. For the catalyst-assisted growth, Fig. 3e–g confirm that both the forked nanoplates (without exfoliation) and the nanobelts have a (010) top surface and a growth direction of [001], while Fig. 3h reveals that the microtower is a layered structure of (010) layers stacked along the [010] direction. Lattice measurements in Fig. 3d and g indicate a planar distance of 0.38 nm for (100) planes and 0.36 nm for (001) planes. These values are slightly smaller than the standard data for $\alpha\text{-MoO}_3$ and the results from XRD measurements. This deviation in lattice parameters may be due to the small error in TEM measurements and the lattice distortion and change from the electron beam irradiation during the TEM examination.²⁵ These results reveal that all the as-synthesized 1D structures have a layered structure consistent with the anisotropic crystal structure of $\alpha\text{-MoO}_3$.^{13b,26}

3.2 Growth evolution and mechanism

The growth process of the 1D MoO_3 rectangular nanoplates without catalysts is similar to the reported CVD growth of 1D WO_3 nanowires,^{23a} in which the refractory metal powders (e.g. Mo and W) were oxidized by heating under an oxygen atmosphere, then oxide vapors were evaporated and transported downstream forming deposition on the substrate at lower temperature. Therefore, the non-catalyst growth of these MoO_3 rectangular nanoplates can be explained by the vapor–solid (VS) growth mechanism,²⁷ as proposed in other vapor phase depositions of MoO_3 belt structures.^{21c,e} On the other hand, as shown in Fig. 2, with the addition of NaOH catalysts, the growth of MoO_3 is greatly enhanced and has two growth stages. To reveal the growth mechanism and the role of the catalysts in the growth, evolution studies were performed on the early stage growth of the forked nanoplates and the second stage growth of the different ultra-long 1D structures.

MoO_3 has a high vapor pressure before the source heating temperature reaches 800 °C, for example, its vapor pressure

is ~76 mTorr at 661 °C.²⁸ The deposition formed during both the temperature ramping and cooling steps will become dominant when the growth time is short. Therefore, the growth evolution for the early stage of the MoO_3 growth cannot be simply performed by reducing the growth time at 800 °C. The production of oxide vapor in our experiments is limited by the oxidation of Mo powders, so the amount of MoO_3 deposition at the early growth stage can be controlled by adjusting the O_2 flow rate. To reveal the initial growth with a small amount of MoO_3 deposition, a series of experiments (as shown in Fig. 4) were performed at different O_2 flow rates, 0.1 sccm, 1 sccm, 3 sccm, and 10 sccm, with a constant growth time of 15 min. To identify the phase change during the growth, micro-Raman spectroscopy was performed on these specimens. The phases were identified by matching the Raman spectra with the Raman patterns reported in the literature.²⁹ The Raman spectra of molybdenum oxide and sodium molybdates are featured with multiple strong peaks located in the high-frequency region from 800 to 1000 cm^{-1} . In this region, the MoO_3 phase shows two peaks with the strongest one at ~820 cm^{-1} ; the $\text{Na}_2\text{Mo}_2\text{O}_7$ phase exhibits five peaks with the strongest one moving to ~937 cm^{-1} , whereas the $\text{Na}_2\text{Mo}_4\text{O}_{13}$ phase has even more peaks at about 819, 841, 898, 915, 962, 970, and 995 cm^{-1} . Detailed matching and comparison of the Raman peaks between the present work and the previous reports are provided in Table S1.† At low O_2 flows, e.g. 0.1 sccm (Fig. 4a) and 1 sccm (Fig. 4d), the MoO_3 deposition shows an island growth with micron-sized particles. The islands grown at 0.1 sccm O_2 were identified as the $\text{Na}_2\text{Mo}_2\text{O}_7$ (i.e., $\text{Na}_2\text{O} \cdot 2\text{MoO}_3$) phase according to their Raman pattern in Fig. 4b. As the O_2 flow increased to 1 sccm, the deposition developed to be the $\text{Na}_2\text{Mo}_4\text{O}_{13}$ (i.e., $\text{Na}_2\text{O} \cdot 4\text{MoO}_3$) phase with a small amount of MoO_3 as revealed by the Raman spectrum in Fig. 4e. This result shows that after the formation of $\text{Na}_2\text{Mo}_4\text{O}_{13}$, MoO_3 started to precipitate underneath the catalyst material. Element analyses in Fig. 4c and f using EDS also confirm the existence of Mo, Na and O in both island depositions. (Note: the Si signals were from the substrates). With further increase of O_2 flow to 1 sccm (Fig. 4g) and 10 sccm (Fig. 4j), the deposition has a morphology of triangular-like particles on top of 1D forked plates. Micro-Raman measurements were carried out on individual particles and plates as shown in Fig. 4h and k. For both specimens, the particles were found to remain in the $\text{Na}_2\text{Mo}_4\text{O}_{13}$ phase with a small amount of the MoO_3 phase from the background, but the plates were identified as the MoO_3 phase. EDS spectra (Fig. 4i and l) also confirmed that the particles had Mo, Na and O, while only Mo and O were present in the plates showing the growth of MoO_3 plate structures. As shown in Fig. 4g and j and previously in Fig. 2, unlike the rectangular nanoplates grown without catalysts, the nanoplates grown with catalysts are highly forked plates with wavy or angled high Miller index surfaces (e.g., in the form of $\{h0l\}$) off the $\{001\}$ planes. With the unsaturated chemical bonds of the surface atoms, these high index surfaces could serve as the growth fronts resulting in a fast growth

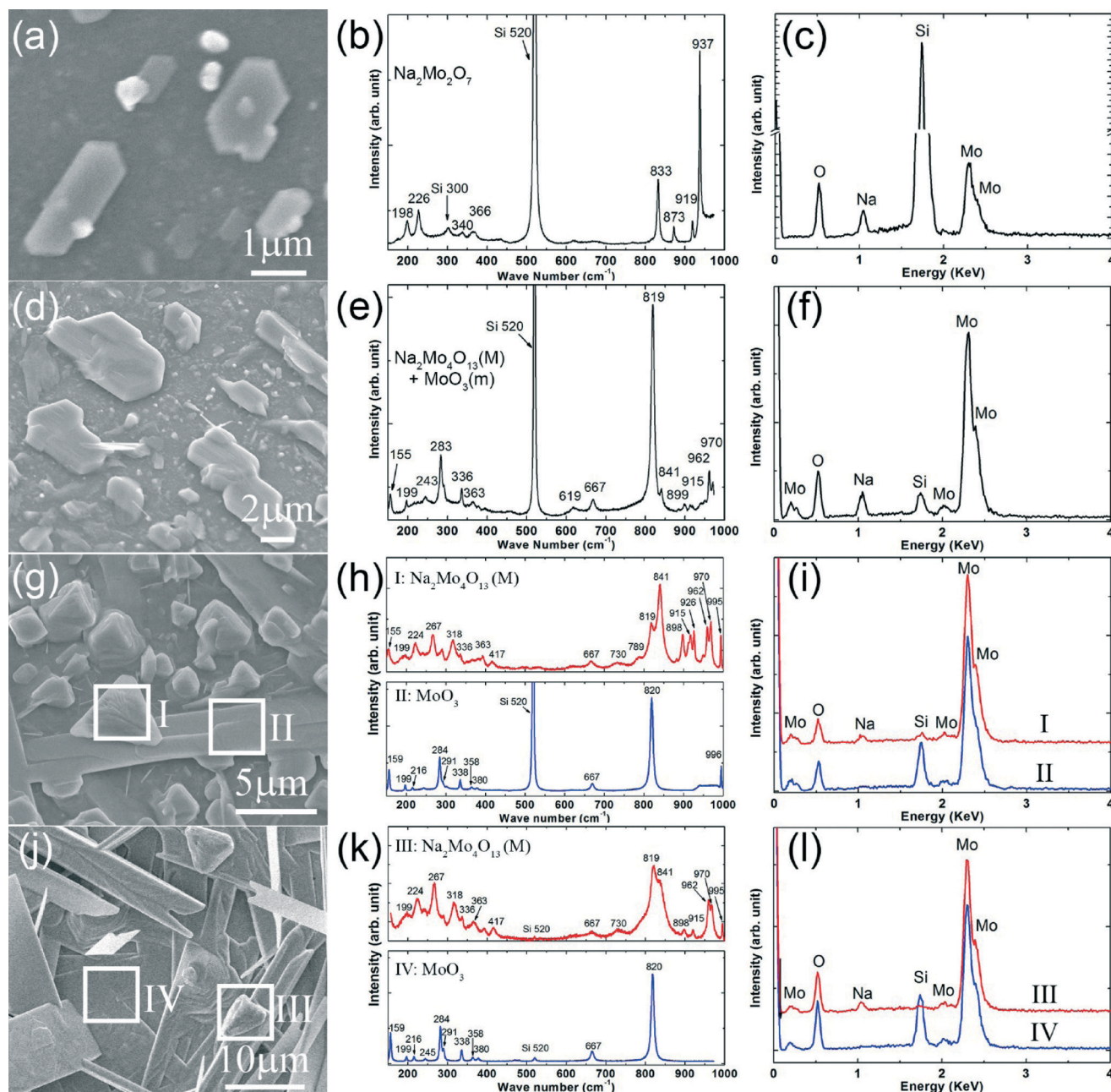


Fig. 4 Growth evolution of the early stage of catalyst-assisted growth of MoO_3 1D structures: SEM images, micro-Raman spectra, and EDS spectra of the specimens grown for 15 min with different O_2 flows: (a–c) 0.1 sccm, (d–f) 1 sccm, (g–i) 3 sccm, and (j–l) 10 sccm. The chemical phases are labeled in the corresponding Raman spectrum, with M denoting majority, and m minority.

along the $\langle 001 \rangle$ direction.^{21a} The forked morphology may be induced by Na^+ doping in the MoO_3 matrix. Na^+ doping in MoO_3 was reported to be able to increase the mobility of Mo^{6+} ions through the MoO_3 lattices.³⁰ This property may also contribute to the enhanced growth of MoO_3 1D structures with NaOH catalysts. However, the absence of Na signals in the EDS spectra (Fig. 4i and l) of the forked MoO_3 nanoplates indicates that the Na^+ doping level in MoO_3 is lower than the detection limit of 0.01 wt% for EDS.³¹

The observed compositional and phase evolutions match the phase diagram of the Na_2MoO_4 – MoO_3 binary system

shown in Fig. 5a.³² During the growth, the NaOH catalysts can directly react with MoO_3 vapor or decompose into Na_2O ³³ and then react with MoO_3 vapor forming sodium molybdates.³⁰ As shown in Fig. 5a, at a typical growth temperature the sodium molybdate phase changes from Na_2MoO_4 to $\text{Na}_2\text{Mo}_2\text{O}_7$, and then to $\text{Na}_2\text{Mo}_4\text{O}_{13}$ with the increase in the supply of MoO_3 vapor. With further increase in MoO_3 composition, the MoO_3 solid phase starts to nucleate and grow while the $\text{Na}_2\text{Mo}_4\text{O}_{13}$ phase remains the same. Since the growth temperature range of 525–300 °C (shaded area on Fig. 5a) for the MoO_3 deposition is mainly below the lowest eutectic temperature of

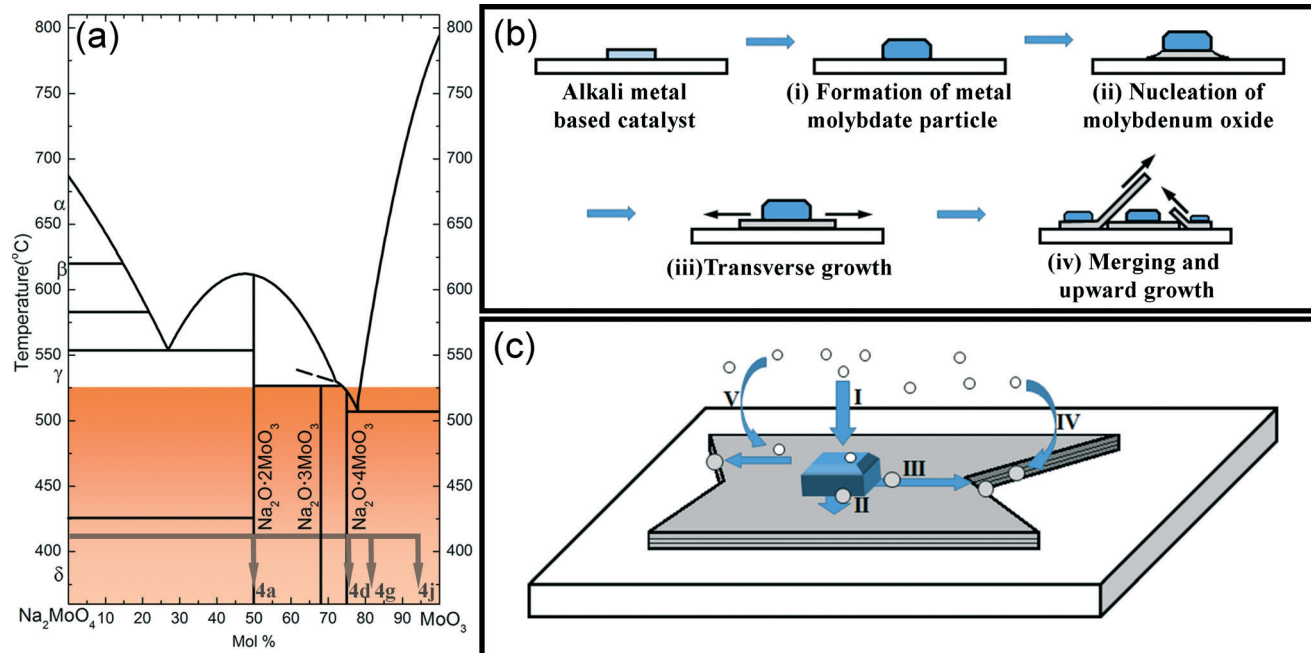


Fig. 5 (a) Na_2MoO_4 - MoO_3 binary phase diagram³² with growth steps indicated showing the early stage evolutions of compositions and phases in Fig. 4. The shadowed area shows the range of the growth temperature. (b-c) Schematic illustrations of (b) growth steps of the VSS growth of MoO_3 nanoplates and (c) atomic processes involved in the VSS mechanism.

~507 $^\circ\text{C}$, the majority of the growth of the MoO_3 plates can be explained as a VSS process. However, the temperature profile of the CVD system was measured at atmospheric pressure without gas flows, while the growth was carried out at low pressures with continuous gas flows. The actual growth temperature on the substrate could be higher than the one indicated by the temperature profile, depending on the pressure and flow rate.³⁴ The heat transfer along the substrate may also affect the temperature on the substrate. Thus, the VSS mechanism here may be the dominant process for the catalyst-assisted growth but the VLS mechanism cannot be totally ruled out, especially for the high growth temperature area. Different from the conventional VSS (and VLS) growth, the most significant feature of the MoO_3 nanoplate growth here is its transverse growth mode in which the growth direction is perpendicular to the catalyst-deposition axis. To explain this unique transverse growth, we propose a modified VSS growth mechanism for the transverse growth of MoO_3 1D structures based on the spreading behavior of MoO_3 . It has been reported in the literature that MoO_3 can spontaneously spread over the surface of supports (e.g., Al_2O_3 , SiO_2 , TiO_2 , and Au) to form a monolayer or submonolayer at a temperature (e.g., 257 $^\circ\text{C}$) well below its melting point of 795 $^\circ\text{C}$.³⁵ The transport of Mo oxide species during the spreading can occur over macroscopic distances, e.g., several hundred microns depending on the temperature and time of the thermal treatments. This strong spreading behavior can be explained by the solid-solid wetting process, in which the dominant driving force is the decrease in total surface free energy.^{35a} Although the detailed transport mechanisms of the spreading are still under debate, it was suggested that the high mobility of the Mo oxide species on substrates and MoO_3 islands can promote the

spreading and the ambient gases could further enhance the spreading.^{35a,c-e} Therefore, the steps of the modified VSS growth are proposed and depicted in Fig. 5b: (i) the catalysts react with MoO_3 vapor forming molybdate particles, (ii) MoO_3 starts to nucleate and form a wetting layer between the particles and the substrate, (iii) as growth continues, more MoO_3 precipitates and spreads laterally leading to the transverse growth of the nanoplates, and (iv) when the nanoplates grow longer and denser, they start to grow upward forming a nanoplate array. Detailed atomic processes involved in the nanoplate growth are illustrated in Fig. 5c. Several pathways can contribute to the growth of MoO_3 nanoplates. MoO_3 vapor is accommodated into the molybdate particles and supersaturated MoO_3 in the molybdate catalysts will precipitate (pathway I). The precipitated MoO_3 may grow at the catalyst-deposition interface (pathway II), or spread along the top surface of MoO_3 (010) and grow at the edges (pathway III). With the strong spreading properties of MoO_3 , the growth *via* pathway III is dominant in our experiments resulting in the transverse growth of the nanoplates. Besides the VSS processes, the transverse growth can be further enhanced *via* the VS processes: (pathway IV) MoO_3 vapor directly condenses onto the growth fronts forming deposition, and (pathway V) MoO_3 vapor adsorbs and diffuses on the (010) surface and produces deposition at the growth fronts. Therefore, the MoO_3 nanoplate growth with alkali metal based catalysts can be explained by the VSS growth mechanism enhanced with the VS mechanism. The transverse growth mode is attributed to the strong spreading capability of MoO_3 . Growth also using alkali metal based catalysts (e.g., KOH and KI) has been reported with $\text{K}_2\text{W}_4\text{O}_{13}$ nanowires and WO_3 nanoribbons and nanosheets.³⁶ However, only the growth temperature slightly

higher than the eutectic temperature was investigated in these reports, and the growth was generally explained by the VLS mechanism. No detailed observation of the location and morphology of the catalyst particles was provided. No transverse growth mode was claimed in these reports and this may be due to the differences in spreading properties between MoO_3 and WO_3 or $\text{K}_2\text{W}_4\text{O}_{13}$.

Growth evolution of the second stage of the MoO_3 growth was investigated at a constant O_2 flow rate of 10 sccm with different growth times, 30 min, 60 min, and 90 min as shown in Fig. 6. Compared to the 15 min growth shown in Fig. 4j, dense arrays of MoO_3 forked nanoplates with a length of hundreds of microns were formed covering the substrate areas at different temperatures (Fig. 6a–d). With the increase in growth time, these nanoplates kept growing and became larger, longer, and denser. Ultra-long 1D MoO_3 structures started to grow on top of the nanoplate arrays. For the growth time of 60 min (Fig. 6e–h), ultra-long nanobelts appeared on top of the nanoplates at the vicinities of 445 °C (Fig. 6f) and 390 °C (Fig. 6g). For the growth time of 90 min, the nanobelts near 445 °C grew longer (Fig. 6j), the nanobelts around 390 °C grew into microbelts (Fig. 6k), and microtowers started

to grow near 340 °C (Fig. 6l). Further growth to 120 min is already displayed in Fig. 2b–g with dense 1D structures of different morphologies.

To reveal the growth mechanisms for the ultra-long 1D structures in the second stage, specimens were carefully examined to locate and identify the catalyst particles (refer to the ESI† for details). Small catalyst particles ranging from several hundred nanometers to several microns were found at different locations of these ultra-long 1D structures (Fig. S2 and S3†). Element analysis (Fig. S2 and S3†) using EDS confirmed the presence of Na, Mo, and O in these particles, indicating that the particles are sodium molybdate catalysts, the same as for the growth of forked nanoplates (Fig. 4g and j). Thus, the growth of these ultra-long 1D structures was also dominated by the VSS mechanism. Two growth modes were proposed and discussed below for different ultra-long structures.

The ultra-long nanobelts and microbelts follow the same transverse growth mode as the one for the forked nanoplates demonstrated in Fig. 5. Growth steps are illustrated in Fig. 7a: catalyst particles could nucleate on the forked nanoplates and promote transverse growth of the nanobelts; as

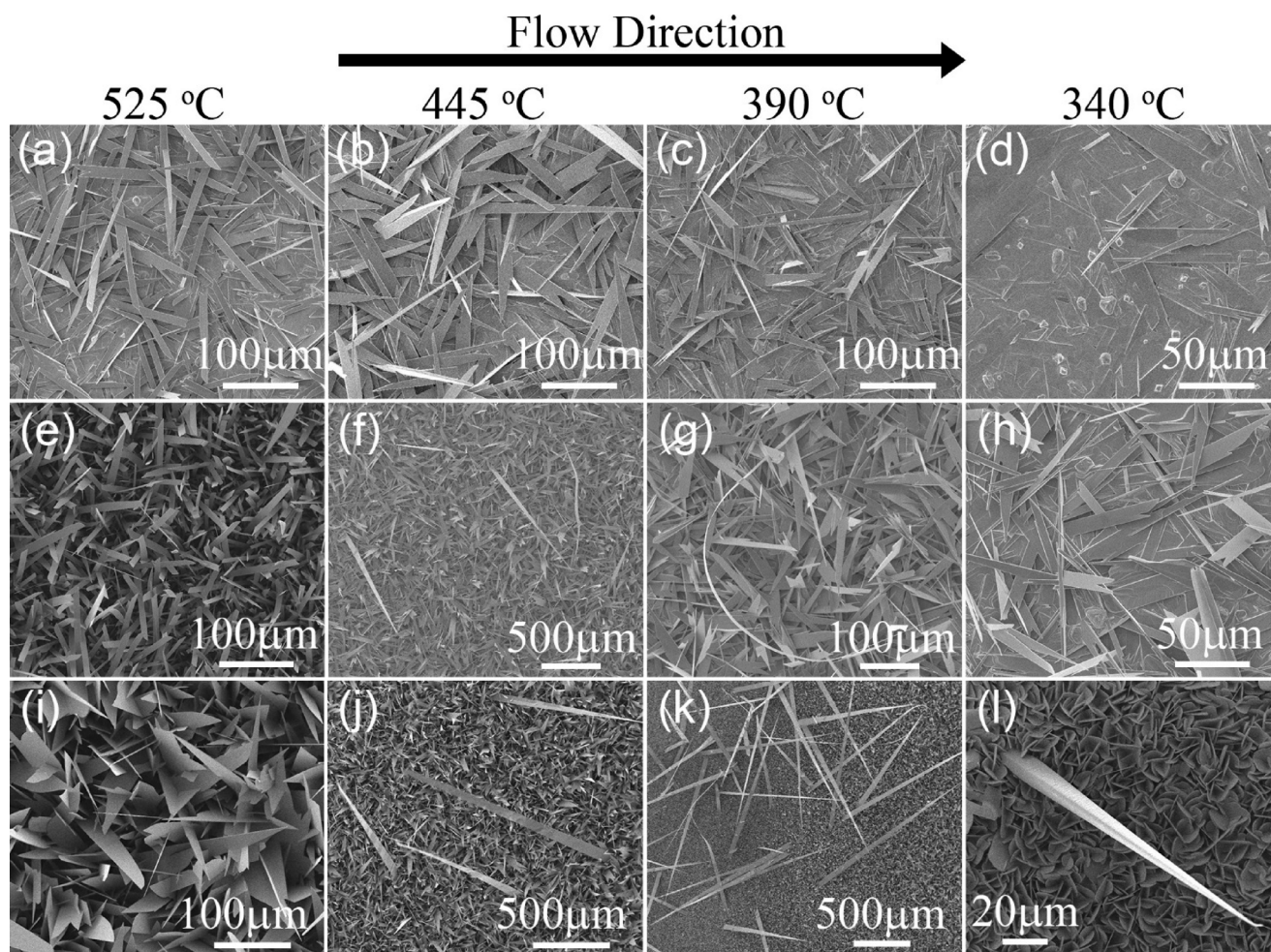


Fig. 6 Growth evolution of the second stage of catalyst-assisted growth of MoO_3 1D structures: SEM images of the deposition at different growth temperatures with growth times of (a–d) 30 min, (e–h) 60 min, and (i–l) 90 min.

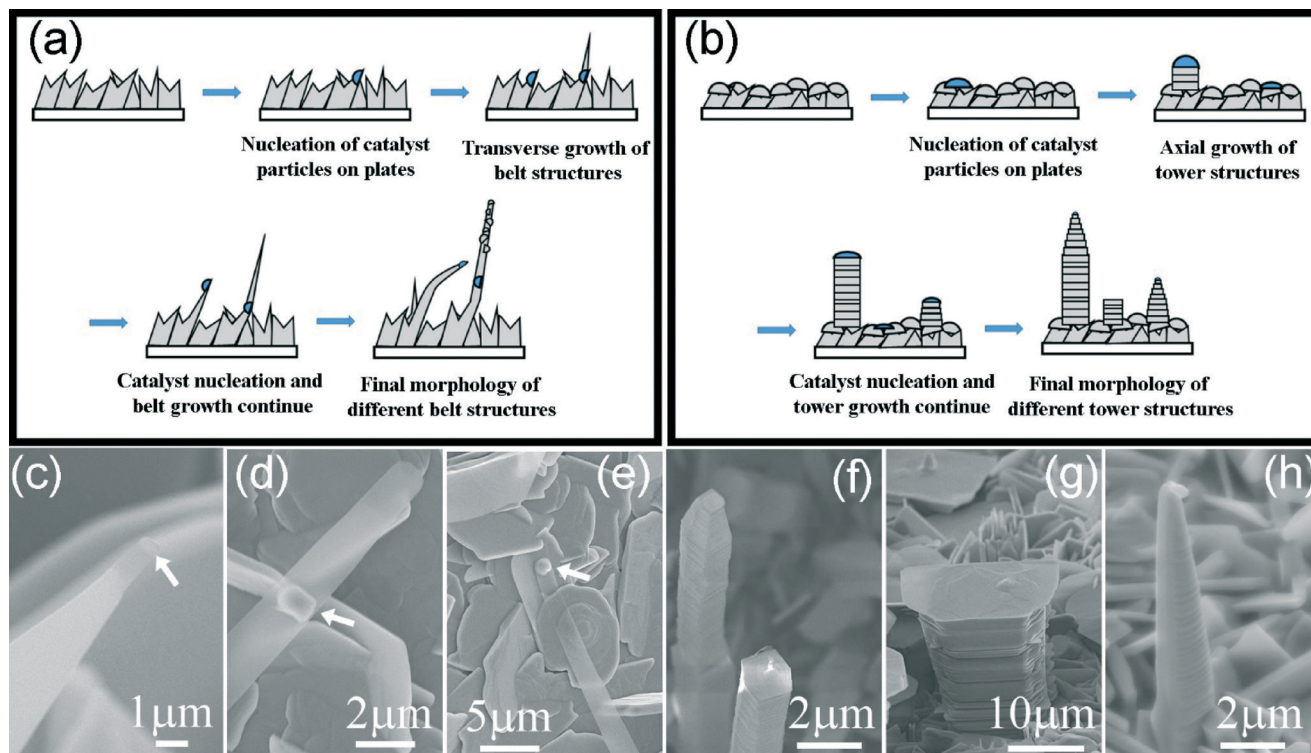


Fig. 7 Schematic illustrations of the VSS growth steps of (a) the transverse mode for MoO_3 nanobelts and microbelts and (b) the axial growth mode for MoO_3 microtowers. (c–e) SEM images of nanobelts showing catalyst particles at different locations: (c) tip of a forked nanoplate, (d) middle of a nanobelt, and (e) tip of a nanobelt. (f–h) SEM images of microtowers with different morphologies: (f) cylinder shape with a tapered tip, (g) flat top, and (h) cone shape.

the catalyst nucleation and the belt growth continue, nanobelts and microbelts with different dimensions will form depending on the growth temperature and growth time. Fig. 7c shows a catalyst particle nucleated at the tip of a forked nanoplate initiating a nanobelt growth. Fig. 7d and e display catalyst particles located at the middle and the tip of two nanobelts, respectively. It is worth noting that the catalyst particles are always present on the side faces of the belt structures. Even when they are located at the tip of the belt structures, they are on the side faces like the “finger nails”. So the growth of the nanobelts and microbelts follows the transverse growth rather than the axial growth. When the belt structures grow into microbelts with micron thickness and millimeter length, dense circular or semicircular nanoflakes (inset of Fig. 2e) grow on top of their side surfaces. This secondary growth on the side surfaces could be attributed to two factors: (1) when the belt structures are so long, stable MoO_3 islands can form on the side surfaces before the oxide species diffuse to the growth front; and (2) as the belt structures grow longer, away from the substrate, the local temperature at the belt surface may be lower than the substrate temperature resulting in slower surface diffusion and quicker vapor condensation. On the other hand, the microtower structures follow the axial growth mode in the conventional VSS process. Low growth temperature may be one of the main reasons for the axial growth of microtowers. First, the microtowers in this study primarily grow at the low temperature

end of the substrate. And as shown in Fig. 6l, the microtowers appear later after a thick layer of nanoplates forms on the substrate. The growth temperature on top of the nanoplate layer could be even lower than the substrate temperature. With a lower growth temperature, the spreading capability of the Mo oxide species is possibly limited. Thus, based on the analysis of atomic processes shown in Fig. 5c, for the microtower structures the transverse growth *via* the pathway III is suppressed and the axial growth *via* the pathway II becomes dominant. Hence, the growth steps of the axial growth of microtowers are demonstrated in Fig. 7b: catalyst particles form on top of the dense and thick nanoplates and lead to the axial growth at the catalyst-deposition interface; with continuous growth and new nucleation of catalyst particles, tower structures with different heights and morphologies can emerge. Fig. 7f–h show the SEM images of microtowers with a tapered tip, flat top, and a cone shape, respectively.

The above growth modes for the second stage growth of ultra-long nanobelts, microbelts, and microtowers are well supported by morphology and compositional analyses. However, to further confirm the proposed growth mechanisms, one essential question has to be answered: how can the catalyst particles nucleate on top of the nanoplates? Considering the low melting temperature of $\text{Na}_2\text{Mo}_4\text{O}_{13}$ (~522 °C) and the low eutectic temperature of the $\text{Na}_2\text{Mo}_4\text{O}_{13}$ – MoO_3 system (~507 °C), it is possible to produce Na-containing vapors in the reaction chamber especially from the high temperature

end of the substrate. The vapors could condense onto the MoO_3 deposition forming catalyst particles and inducing the VSS growth in the second stage. Since no data about $\text{Na}_2\text{Mo}_4\text{O}_{13}$ vapor pressures are available, “side-by-side” growth (refer to the ESI†) was performed to verify the above hypothesis. Two substrates, one with NaOH catalysts and one bare substrate, were loaded side-by-side at the same location for the growth (Fig. S4a†). To avoid any possible catalyst transports through surface diffusion, the two substrates were separated with a gap of several millimeters. After the growth, besides the non-catalyst rectangular plates, catalyst induced 1D structures (including forked nanoplates, nanobelts, microbelts, and microtowers) were also found on the bare substrate (Fig. S4b–i†). This result clearly confirms that the catalyst materials can be evaporated and transferred from the NaOH treated substrate to the untreated one. The catalyst vapors can nucleate and form catalyst particles on the MoO_3 deposition promoting the VSS growth of different 1D structures. It is worth mentioning that catalyst particles were not observed on all the 1D structures. This fact can be explained by the following reasons. (1) Catalyst particles can nucleate at any locations along the 1D structures. Some particles may be invisible hiding on the backside of the 1D structures. (2) Because of evaporation, the catalyst particles may become too small or too thin to be detected. Some particles could even totally disappear terminating the catalyzed growth, which may explain the growth of the microtowers with a flat top (Fig. 2f and 7g). The evaporation and nucleation of catalyst materials not only promote the growth of the 1D structures in the second stage growth, but also play important roles in shaping the morphologies of these 1D structures. Many 1D structures in the second stage were found to have a tapered shape, such as triangular nanobelts (Fig. 2b and d) and microbelts (Fig. 6k), microtowers with tapered tips (Fig. 2f and 7f) and cone-shaped microtowers (Fig. 7h). Several factors can contribute to the tapering of the 1D structures. First, the reduction in catalyst size may induce the tapering.³⁷ Due to evaporation, the size of the catalyst particles can shrink during the growth resulting in the tapered growth. The VS growth on the side surfaces is another possible mechanism,^{3b,38} which promotes the radial growth of the 1D structures forming the tapered shape. Another important factor is the gradually reduced growth during the cooling process. During the cooling, the MoO_3 vapor supply and the growth temperature gradually decrease. Hence the growth rate slows down producing the tapered tips on top of some 1D structures.

3.3 Different catalysts, hierarchical structures, and optical properties

With similar phase diagrams like the $\text{Na}_2\text{Mo}_4\text{O}_{13}$ – MoO_3 binary phase diagram, materials that contain other alkali metals, such as Li and K,³² can also be used as catalysts for the growth of MoO_3 1D structures. Experiments have been performed with a variety of alkali metal based materials, including KI, Na_2CO_3 , and even alkali metal containing

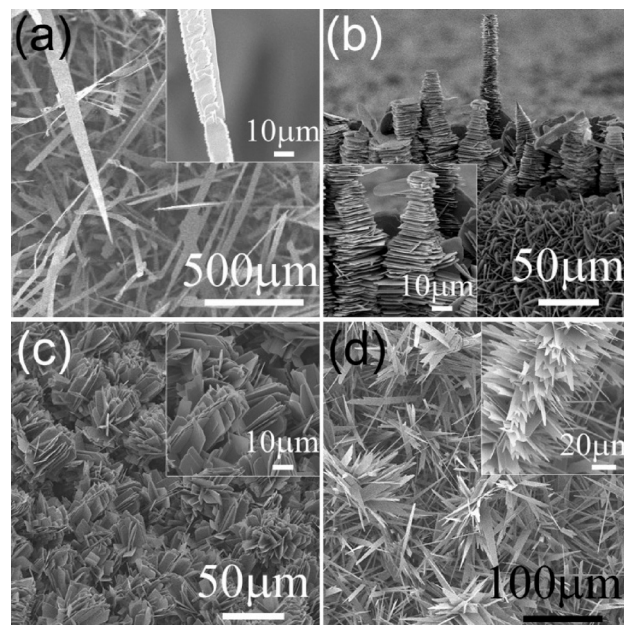


Fig. 8 SEM images of selected MoO_3 1D structures: (a) nanobelts grown with KI and (b) microtowers grown on ITO glass; and (c–d) examples of hierarchical MoO_3 1D structures grown by multiple-growth.

substrates, such as ITO coated glass, glass, and mica. Some selected 1D structures using KI and ITO glass are shown in Fig. 8a and b, respectively. Other examples are shown in Fig. S5†. Based on the modified VSS growth mechanism, hierarchical structures have also been achieved *via* multiple-growth approaches. Two examples of the hierarchical structures are demonstrated in Fig. 8c and d. Fig. 8c shows a specimen grown without catalysts for 120 min followed by a second growth with NaI for 30 min. Assemblies of nanoplates with perpendicular plate surfaces and parallel growth direction were formed. Fig. 8d demonstrates another specimen grown with NaOH catalysts for 30 min followed by another growth of 15 min without any additional treatment. The resulting hierarchical structures have a “test-tube-brush” structure with nanoplate branches grown perpendicular around the primary nanoplate stems.

At last, optical properties of the MoO_3 deposition were studied using UV-vis spectroscopy. The absorption spectrum is presented in Fig. S6† showing that the absorption edge of the MoO_3 crystals obtained in this work, at around 3.0 eV, resembles those of previous reports on single crystalline and thin film MoO_3 in the literature.³⁹ The linear fitting (inset of Fig. S6†) of the logarithmic plot of the absorbance at the absorption edge indicates a low-energy tail following Urbach’s rule, presumably due to bound exciton induced transition and lattice imperfection caused energy band distortion.³⁹

4 Conclusions

In summary, MoO_3 1D structures were synthesized using alkali metal based catalysts. The MoO_3 growth was greatly enhanced by the presence of the catalysts forming forked

nanoplates and ultra-long 1D structures, such as nanobelts, microbelts, and microtowers. The VSS process was identified as the dominant growth mechanism. Different from the conventional catalyst-assisted mechanisms, the new transverse growth mode and conventional axial growth mode were discovered. With the thorough study of the growth evolution, a modified VSS mechanism was proposed based on the strong spreading behavior of the MoO₃ material. The proposed mechanism successfully explained the new growth modes. Based on this mechanism, the growth of MoO₃ layered 1D structures was realized using a variety of alkali metal based catalysts, and hierarchical structures were achieved by multiple-growth approaches. We believe that the 1D growth using alternative catalysts provides promising opportunities to extend the catalyst-assisted 1D growth to a much broader scope. The growth mechanism revealed here provides a new approach to control the growth direction of 1D structures with respect to the catalyst-deposition axis and can be applied to other layered materials with similar spreading properties to MoO₃.

Acknowledgements

This work was supported by National Science Foundation (DMR-1006547), the start-up fund from the Department of Mechanical Engineering and Engineering Science (MEES) and Charlotte Research Institute at the University of North Carolina at Charlotte (UNC Charlotte), and the faculty research grant from UNC Charlotte. The authors appreciate the Department of MEES and the Center for Optoelectronics and Optical Communications at UNC Charlotte for the support in using multiuser facilities. Y. Z. acknowledges the support of Bissell Distinguished Professorship.

Notes and references

- (a) R. S. Wagner and W. C. Ellis, *Appl. Phys. Lett.*, 1964, **4**, 89; (b) E. I. Givargizov, *J. Cryst. Growth*, 1975, **31**, 20.
- (a) C. M. Lieber, *Solid State Commun.*, 1998, **107**, 607; (b) M. Law, J. Goldberger and P. D. Yang, *Annu. Rev. Mater. Res.*, 2004, **34**, 83; (c) Y. N. Xia, P. D. Yang, Y. G. Sun, Y. Y. Wu, B. Mayers, B. Gates, Y. D. Yin, F. Kim and Y. Q. Yan, *Adv. Mater.*, 2003, **15**, 353; (d) H. J. Fan, P. Werner and M. Zacharias, *Small*, 2006, **2**, 700.
- (a) T. I. Kamins, R. S. Williams, D. P. Basile, T. Hesjedal and J. S. Harris, *J. Appl. Phys.*, 2001, **89**, 1008; (b) Y. Wang, V. Schmidt, S. Senz and U. Goesele, *Nat. Nanotechnol.*, 2006, **1**, 186; (c) J. L. Lensch-Falk, E. R. Hemesath, D. E. Perea and L. J. Lauhon, *J. Mater. Chem.*, 2009, **19**, 849.
- (a) H. F. Yan, Y. J. Xing, Q. L. Hang, D. P. Yu, Y. P. Wang, J. Xu, Z. H. Xi and S. Q. Feng, *Chem. Phys. Lett.*, 2000, **323**, 224; (b) L. W. Yu, P. J. Alet, G. Picardi and P. R. I. Cabarrocas, *Phys. Rev. Lett.*, 2009, **102**; (c) H. Chandrasekaran, G. U. Sumanasekara and M. K. Sunkara, *J. Phys. Chem. B*, 2006, **110**, 18351.
- (a) T. J. Trentler, K. M. Hickman, S. C. Goel, A. M. Viano, P. C. Gibbons and W. E. Buhro, *Science*, 1995, **270**, 1791; (b) T. Hanrath and B. A. Korgel, *J. Am. Chem. Soc.*, 2002, **124**, 1424.
- (a) J. D. Holmes, K. P. Johnston, R. C. Doty and B. A. Korgel, *Science*, 2000, **287**, 1471; (b) F. M. Davidson, R. Wiacek and B. A. Korgel, *Chem. Mater.*, 2005, **17**, 230.
- (a) H. Y. Tuan, D. C. Lee, T. Hanrath and B. A. Korgel, *Nano Lett.*, 2005, **5**, 681; (b) S. Barth, M. M. Kolesnik, K. Donegan, V. Krstic and J. D. Holmes, *Chem. Mater.*, 2011, **23**, 3335.
- Z. W. Pan, Z. R. Dai, C. Ma and Z. L. Wang, *J. Am. Chem. Soc.*, 2002, **124**, 1817.
- Z. W. Pan, S. Dai, C. M. Rouleau and D. H. Lowndes, *Angew. Chem., Int. Ed.*, 2005, **44**, 274.
- J. L. Wang, K. M. Chen, M. Gong, B. Xu and Q. Yang, *Nano Lett.*, 2013, **13**, 3996–4000.
- K. W. Kolasinski, *Curr. Opin. Solid State Mater. Sci.*, 2006, **10**, 182.
- (a) S. A. Fortuna, J. Wen, I. S. Chun and X. Li, *Nano Lett.*, 2008, **8**, 4421; (b) S. Li, X. Huang, Q. Liu, X. Cao, F. Huo, H. Zhang and C. L. Gan, *Nano Lett.*, 2012, **12**, 5565; (c) Z. Zhang, L. M. Wong, H. X. Wang, Z. P. Wei, W. Zhou, S. J. Wang and T. Wu, *Adv. Funct. Mater.*, 2010, **20**, 2511.
- (a) F. Cora, A. Patel, N. M. Harrison, C. Roetti and C. R. A. Catlow, *J. Mater. Chem.*, 1997, **7**, 959; (b) M. Chen, U. V. Waghmare, C. M. Friend and E. Kaxiras, *J. Chem. Phys.*, 1998, **109**, 6854.
- J. N. Yao, K. Hashimoto and A. Fujishima, *Nature*, 1992, **355**, 624.
- P. E. Sheehan and C. M. Lieber, *Science*, 1996, **272**, 1158.
- Y. Chen, C. Lu, L. Xu, Y. Ma, W. Hou and J.-J. Zhu, *CrystEngComm*, 2010, **12**, 3740.
- (a) E. Comini, L. Yubao, Y. Brando and G. Sberveglieri, *Chem. Phys. Lett.*, 2005, **407**, 368; (b) A. M. Taurino, A. Forleo, L. Francioso, P. Siciliano, M. Stalder and R. Nesper, *Appl. Phys. Lett.*, 2006, **88**, 152111; (c) X. Sha, L. Chen, A. C. Cooper, G. P. Pez and H. Cheng, *J. Phys. Chem. C*, 2009, **113**, 11399; (d) S. Choopun, P. Mangkorntong, P. Subjareon, N. Mangkorntong, H. Tabata and T. Kawai, *Jpn. J. Appl. Phys., Part 2*, 2004, **43**, L91–L93.
- L. Q. Mai, B. Hu, W. Chen, Y. Y. Qi, C. S. Lao, R. S. Yang, Y. Dai and Z. L. Wang, *Adv. Mater.*, 2007, **19**, 3712.
- S. Hariharan, K. Saravanan and P. Balaya, *Electrochem. Commun.*, 2013, **31**, 5.
- (a) X.-L. Li, J.-F. Liu and Y.-D. Li, *Appl. Phys. Lett.*, 2002, **81**, 4832; (b) T. Xia, Q. Li, X. Liu, J. Meng and X. Cao, *J. Phys. Chem. B*, 2006, **110**, 2006; (c) G. Li, L. Jiang, S. Pang, H. Peng and Z. Zhang, *J. Phys. Chem. B*, 2006, **110**, 24472; (d) G. A. Camacho-Bragado and M. Jose-Yacamán, *Appl. Phys. A: Mater. Sci. Process.*, 2006, **82**, 19.
- (a) H. C. Zeng, *J. Cryst. Growth*, 1998, **186**, 393; (b) J. Li, P. Wei, J. Chen and L. Rongti, *J. Am. Ceram. Soc.*, 2002, **85**, 2116; (c) Y. B. Li, Y. Bando, D. Golberg and K. Kurashima, *Appl. Phys. Lett.*, 2002, **81**, 5048; (d) J. Zhou, S. Z. Deng, N. S. Xu, J. Chen and J. C. She, *Appl. Phys. Lett.*, 2003, **83**, 2653; (e) P. Badica, *Cryst. Growth Des.*, 2007, **2**; (f) B. Yan, Z. Zheng, J. Zhang, H. Gong, Z. Shen, W. Huang and T. Yu, *J. Phys. Chem. C*, 2009, 20259.

- 22 L. Cai, P. M. Rao and X. Zheng, *Nano Lett.*, 2011, **11**, 872.
- 23 (a) H. Zhang, T. T. Xu, M. Tang, T.-H. Her and S.-Y. Li, *J. Vac. Sci. Technol., B*, 2010, **28**, 310; (b) T. Sheng, P. P. Chavvakula, B. Cao, N. Yue, Y. Zhang and H. Zhang, *J. Cryst. Growth*, 2014, **395**, 61.
- 24 K. Kalantar-zadeh, J. Tang, M. Wang, K. L. Wang, A. Shailos, K. Galatsis, R. Kojima, V. Strong, A. Lech and R. B. K. De, *Nanoscale*, 2010, 429.
- 25 D. E. Diaz-Droguett, A. Zuniga, G. Solorzano and V. M. Fuenzalida, *J. Nanopart. Res.*, 2012, **14**, 679.
- 26 F. Cora, A. Patel, N. M. Harrison, C. Roetti, C. Richard and A. Catlow, *J. Mater. Chem.*, 1997, **7**, 959.
- 27 Z. R. Dai, Z. W. Pan and Z. L. Wang, *Adv. Funct. Mater.*, 2003, **13**, 9.
- 28 *The Oxide Handbook*, ed. G. V. Samsonov, IFI/Plenum, New York, 1973.
- 29 (a) G. D. Saraiva, W. Paraguassu, M. Maczka, P. T. C. Freire, F. F. de Sousa and J. Mendes Filho, *J. Raman Spectrosc.*, 2011, **42**, 1114; (b) V. V. Fomichev, M. E. Poloznikova and O. I. Kondratov, *Russ. Chem. Rev.*, 1992, **61**, 877; (c) K. Schofield, *Energy Fuels*, 2005, **19**, 1898; (d) K. Eda, *J. Solid State Chem.*, 1991, **95**, 64; (e) W. G. Chu, L. N. Zhang, H. F. Wang, Z. H. Han, D. Han, Q. Q. Li and S. S. Fan, *J. Mater. Res.*, 2007, **22**, 1609–1617; (f) T. Siciliano, A. Tepore, E. Filippo, G. Micocci and M. Tepore, *Mater. Chem. Phys.*, 2009, **114**, 687.
- 30 G. A. El-Shobaky, G. A. Fagal and N. A. Hassan, *Thermochim. Acta*, 1998, **311**, 205.
- 31 J. Goldstein, *Scanning electron microscopy and X-ray microanalysis*, Kluwer Academic/Plenum Publishers, New York, 2003.
- 32 (a) E. M. Levin, *Phase diagrams for ceramists*, American Ceramic Society, Columbus, Ohio, 1956; (b) F. Hoermann, *Z. Anorg. Allg. Chem.*, 1929, **177**, 145.
- 33 V. P. Yurkinskii, E. G. Firsova and S. A. Proskura, *Russ. J. Appl. Chem.*, 2005, **78**, 360.
- 34 K. Subannajui, N. Ramgir, R. Grimm, R. Michiels, Y. Yang, S. Muller and M. Zacharias, *Cryst. Growth Des.*, 2010, **10**, 1585.
- 35 (a) J. Leyrer, D. Mey and H. Knözinger, *J. Catal.*, 1990, **124**, 349; (b) S. Gunther, M. Marsi, A. Kolmakov, M. Kiskinova, M. Noeske, E. Taglauer, G. Mestl, U. A. Schubert and H. Knozinger, *J. Phys. Chem. B*, 1997, **101**, 10004; (c) W. M. Xu, J. F. Yan, N. Z. Wu, H. X. Zhang, Y. C. Xie, Y. Q. Tang and Y. F. Zhu, *Surf. Sci.*, 2000, **470**, 121; (d) Z. Song, T. Cai, Z. Chang, G. Liu, J. A. Rodriguez and J. Hrbek, *J. Am. Chem. Soc.*, 2003, **125**, 8059; (e) S. Gunther, L. Gregoratti, M. Kiskinova, E. Taglauer, P. Grotz, U. A. Schubert and H. Knozinger, *J. Chem. Phys.*, 2000, **112**, 5440.
- 36 (a) H. Qi, C. Wang and J. Liu, *Adv. Mater.*, 2003, **15**, 411; (b) K. Q. Hong, W. C. Yin, H. S. Wu, J. Gao and M. H. Xie, *Nanotechnology*, 2005, **16**, 1608; (c) R. Hu, H. Wu and K. Hong, *J. Mater. Res.*, 2009, **24**, 187.
- 37 (a) J. B. Hannon, S. Kodambaka, F. M. Ross and R. M. Tromp, *Nature*, 2006, **440**, 69; (b) E. J. Schwalbach and P. W. Voorhees, *Nano Lett.*, 2008, **8**, 3739.
- 38 S. S. Amin, A. W. Nicholls and T. T. Xu, *Nanotechnology*, 2007, **18**.
- 39 (a) S. K. Deb, *Proc. R. Soc. London, Ser. A*, 1968, **304**, 211; (b) M. Itoh, K. Hayakawa and S. Oishi, *J. Phys.: Condens. Matter*, 2001, **13**, 6853.